6179

Machine learning–spatial quantification of the tumor microenvironment identifies differences associated with response to bintrafusp alfa vs. pembrolizumab treatment in the Phase 3 INTR@PID Lung 037 study

John Abel[1*], Andreas Machl[2], Aslihan Gerhold-Ay[3], Limin Yu[1], Darpan Sanghavi[1], Ben Trotter[1], Neel Patel[1], Ylaine Gerardin[1], Ramprakash Srinivasan[4], Sergine Brutus[5], Thomas Mrowiec[3]

[1]PathAI, Boston, MA, USA; [2]EMD Serono, Billerica, MA, USA; [3]the healthcare business of Merck KGaA, Darmstadt, Germany; [4]Calico Life Sciences, South San Francisco, CA, USA; [5]Mass General Brigham, Sommerville, MA, USA.

*Presenting author (john.abel@pathai.com)

CONCLUSIONS

- **Overall, human-interpretable features and immunophenotyping facilitated response prediction to bintrafusp alfa and pembrolizumab, identifying differences in patient populations benefiting from treatment.**
- **Pembrolizumab response was greater for immune-inflamed tumors, whereas the bintrafusp alfa response was associated with macrophage infiltration of the tumor stroma.**
- **Machine learning–based spatial analysis of the TME shows promise for immunotherapy biomarker discovery and validation.**

INTRODUCTION

- Machine learning digital pathology models can accurately quantify predictive biomarkers such as PD-L1.[1]
- Here, tissue-conserving machine learning assessment of the TME in H&E-stained whole-slide images was combined with RNA sequencing for high-dimensional TME quantification for biomarker discovery.
- The orthogonal methods were applied to a retrospective analysis of a randomized Phase 3 trial directly comparing two immunotherapeutics, anti-PD-1 pembrolizumab and bintrafusp alfa, a first-in-class bifunctional fusion protein composed of the extracellular domain of TGF-βRII (a TGF-β "trap") fused to a human IgG1 monoclonal antibody blocking PD-L1. In this phase 3 study, patients with advanced non-small cell lung cancer and high PD-L1 expression failed to demonstrate superior efficacy of first-line bintrafusp alfa over pembrolizumab.[2]

METHODS

Machine learning models

- Non-small cell lung cancer machine learning models previously trained to exhaustively quantify cell types and tissue regions in H&E-stained tissue were refined and deployed on 273 whole-slide images from 251 cases (bintrafusp alfa, n=130; pembrolizumab, n=121) from INTR@PID Lung 037/ NCT03631706.
- Human-interpretable features describing the complex spatial organization of different cell types and tissue regions in the TME were extracted from model predictions (**Figure 1**) and used for further analyses.

Figure 1. Human-interpretable feature extraction from model predictions

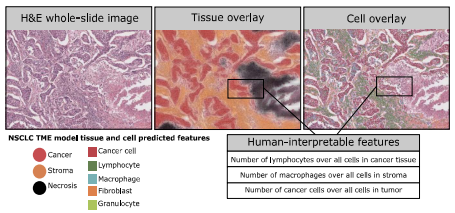

Dataset

- We deployed the model on all 273 available images associated with the study. The resulting feature table was QCed to eliminate features and cases with excessive missing data. This process included focusing on intensive variables that are not a function of size of tissue sample size and exclusion of samples with limited or missing features relevant to this study. Ultimately, this QC yielded a final dataset of 200 features for each of the 251 cases (bintrafusp alfa, n=130; pembrolizumab, n=121). Detailed demographics and baseline characteristics of the patient population has been previously published.[2]

Human-interpretable feature analyses

- Human-interpretable features were selected for analysis and grouped into five clusters using K-means consensus clustering (**Table 1**) to describe the frequency of lymphocytes in the cancer epithelium; frequency of macrophages, fibroblasts, and granulocytes in the stroma; and the abundance of cancer cells relative to all other cells in the tumor.
  - Consensus clustering – Consensus clustering was used as described in the literature[3] to identify stable feature clusters.
  - K-means clustering (scikit-learn implementation) was applied with 80% subsampling of features and 80% subsampling of cases for 300 permutations to construct feature coincidence matrices. K was varied between 2 and 10.
  - The PAC was computed for each of the K resulting coincidence matrices. PAC, for a coincidence matrix was defined as the difference between the value of the cumulative distribution function of the coincidence matrix at coincidences of 0.9 and 0.1.
  - The PAC, representing the proportion of features clustering between 10% and 90% of permutations, was locally minimized over K to identify the K with the fewest features exhibiting ambiguity in clustering.

Table 1. Human-interpretable feature clusters

Cluster 0	Granulocyte features	Cluster 3	Cancer features
Cluster 1	Lymphocyte features	Cluster 4	Fibroblast features
Cluster 2	Macrophage features		

- Bulk RNA sequencing was performed for 186 samples, yielding 177 whole-slide image–RNA sequencing pairs.
- Spearman correlation between human-interpretable features and gene expression or signature was calculated. Top gene associations were analyzed via gene set enrichment analysis (**Table 2**).
- Human-interpretable features were used for immunophenotyping (immune-excluded, inflamed, and desert) via prespecified cutoffs (following pathologist recommendations) on tumor-infiltrating lymphocyte abundance, and for biomarker discovery via Cox modeling of PFS and OS.
- Top two associated gene sets for each human-interpretable feature cluster describing immune cell abundance.

RESULTS

- Gene expression and signatures were associated with human-interpretable features that quantified immune spatial abundance in TME (e.g., cancer epithelium vs. immune checkpoint signature[3]; **Table 2**).
- Immune-excluded, immune-inflamed, and immune-desert phenotypes for pembrolizumab were 70.1%, 26.3%, and 3.6%, respectively.

Table 2. Association of gene expression and signatures with human-interpretable feature clusters

Human-interpretable feature cluster	Gene set description	Genes in overlap/ total genes	P-value	Q-value*
Lymphocyte abundance	Cytokine signaling in immune system	66/729	<0.001	<0.001
	Adaptive immune system	67/829	<0.001	<0.001
Granulocyte abundance	Innate immune system	19/1124	<0.001	<0.001
	Neutrophil degranulation	11/479	<0.001	<0.001
Macrophage abundance	Extracellular matrix organization	55/300	<0.001	<0.001
	Integrin cell surface interactions	23/85	<0.001	<0.001

*Adjusted p-values by false discovery rate.

- Improved PFS and OS were associated with an immune-inflamed phenotype for pembrolizumab (PFS, HR=0.36, p=0.007, 95% CI: 0.17–0.75; OS, HR=0.37, p=0.065, 95% CI: 0.13–1.06; **Figure 2** and **Table 3**).

Figure 2. (A) Association of immune phenotypes with PFS for pembrolizumab. (B) Association of immune phenotypes with OS for pembrolizumab

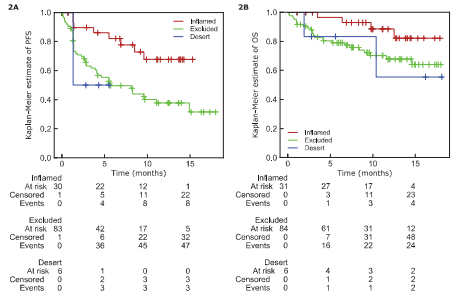

Table 3. Association of immune phenotypes with PFS and OS for pembrolizumab

	Median survival, months (95% CI)	6-month survival rate, %	12-month survival rate, %	24-month survival rate, %	HR (95% CI)	P-value
PFS						
Inflamed (n=30)	Inf (9.6–inf)	82%	68%	68%	0.36 (0.17–0.75)	0.007
Excluded (n=83)	5.7 (3.9–11.1)	50%	38%	31%	2.19 (1.14–4.23)	0.019
Desert (n=6)	Inf (1.3–inf)	50%	50%	50%	1.76 (0.54–5.69)	0.346
OS						
Inflamed (n=31)	Inf (inf–inf)	96%	88%	82%	0.37 (0.13–1.06)	0.065
Excluded (n=83)	Inf (14.6–inf)	79%	68%	64%	2.07 (0.84–5.07)	0.112
Desert (n=6)	Inf (1.9–inf)	83%	56%	56%	1.43 (0.34–6.0)	0.627

- In interaction with bintrafusp alfa, stromal macrophages were associated with improved survival (PFS, HR=0.72, p=0.062, 95% CI: 0.50–1.02; shown in **Table 4** and OS, HR=0.62, p=0.058, 95% CI: 0.38–1.02).

Table 4: Correlation of human-interpretable feature clusters with PFS

Covariate (Human-interpretable feature, arm, or human-interpretable feature arm interaction)	HR (95% CI)	P-value
Fraction of granulocyte cells over all cells in stromal tissue	0.99 (1.28–0.77)	0.961
Bintrafusp alfa_pembrolizumab	1.21 (1.71–0.85)	0.292
Bintrafusp alfa x fraction of granulocyte cells over all cells in stromal tissue	1.02 (1.44–0.72)	0.914
Fraction of lymphocyte cells over all cells in cancer tissue	0.65 (0.86–0.50)	0.002
Bintrafusp alfa_pembrolizumab	1.25 (1.79–0.88)	0.218
Bintrafusp alfa x fraction of lymphocyte cells over all cells in cancer tissue	1.38 (1.96–0.97)	0.070
Fraction of macrophage cells over all cells in stromal tissue	1.20 (1.54–0.93)	0.161
Bintrafusp alfa_pembrolizumab	1.21 (1.72–0.85)	0.285
Bintrafusp alfa x fraction of macrophage cells over all cells in stromal tissue	0.72 (0.50–1.02)	0.062
Fraction of cancer cells over all cells in tumor tissue	1.17 (1.55–0.88)	0.280
Bintrafusp alfa_pembrolizumab	1.22 (1.73–0.86)	0.269
Bintrafusp alfa x fraction of cancer cells over all cells in tumor tissue	1.03 (1.51–0.71)	0.862
Fraction of fibroblasts cells over all cells in stromal tissue	1.12 (1.50–0.84)	0.429
Bintrafusp alfa_pembrolizumab	1.23 (1.75–0.86)	0.250
Bintrafusp alfa x fraction of fibroblasts cells over all cells in stromal tissue	1.03 (1.51–0.70)	0.879

- PFS and OS were comparable between treatment arms in immune-excluded cases (pembrolizumab vs. bintrafusp alfa: PFS, HR=0.93, p=0.73, 95% CI: 0.63–1.39; OS, HR=1.09, p=0.77, 95% CI: 0.62–1.92; **Figure 3** and **Table 5**).

Figure 3. (A) PFS of immune-excluded cases treated with pembrolizumab vs. bintrafusp alfa. (B) OS of immune-excluded cases treated with pembrolizumab vs. bintrafusp alfa

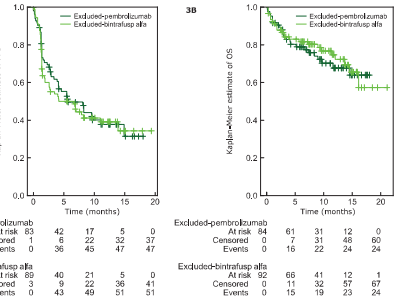

Table 5: PFS and OS of immune-excluded cases treated with pembrolizumab and bintrafusp alfa

	Median survival, months (95% CI)	6-month survival rate, %	12-month survival rate, %	24-month survival rate, %	HR (95% CI)	P-value
PFS						
Pembrolizumab (n=83)	5.7 (3.9–11.1)	50%	38%	31%	0.93 (0.63–1.39)	0.733
Bintrafusp alfa (n=89)	6.6 (1.9–13.9)	50%	39%	34%	1.07 (0.72–1.59)	0.733
OS						
Pembrolizumab (n=84)	Inf (4.6–inf)	79%	68%	64%	1.09 (0.62–1.92)	0.767
Bintrafusp alfa (n=92)	Inf (16.1–inf)	82%	72%	57%	0.92 (0.52–1.62)	0.767

Abbreviations: CI, confidence interval; **H&E,** hematoxylin and eosin; **HR,** hazard ratio; **IgG1,** immunoglobulin G1; **Inf,** Infinity; **OS;** overall survival; **PAC,** proportion of ambiguous clustering; **PD-1,** programmed cell death 1; **PD-L1,** programmed cell death ligand 1; **PFS,** progression-free survival, **RNA,** ribonucleic acid; **TGF-βRII,** transforming growth factor-β receptor II; **TME,** tumor microenvironment.

References: 1. Baxi V, et al. *Modern Pathology*. 2022;35(11):23–32. **2.** Cho BC, et al. *Journal of Thoracic Oncology*. 2023;18(12):1731–1742. **3.** Mariathasan S, et al. *Nature*. 2018;554(7693):544–548.

Acknowledgements: The authors would like to thank patients and their families, investigators, co-investigators, and the study teams at each of the participating centers and at the healthcare business of Merck KGaA, Darmstadt, Germany. This study was sponsored by the healthcare business of Merck KGaA, Darmstadt, Germany (CrossRef Funder ID: 10.13039/100009945). Medical writing assistance was provided by Satrupa Das, PhD, CMPP (Merck Specialties Pvt. Ltd, Bengaluru, India, an affiliate of Merck KGaA, Darmstadt, Germany).

Disclosures: JA, LY, DS, BT, NP, and **YG,** are employees of PathAI Inc, **RS** is a former employee of PathAI Inc, and owns stocks in PathAI Inc, **SB** is a former employee of PathAI Inc, and owns stocks in PathAI Inc, **AM** is employed by EMD Serono, **AG-A** and **TM** are employed by the healthcare business of Merck KGaA, Darmstadt, Germany.

Presented at the American Association for Cancer Research Annual Meeting 2024 | April 5–10, 2024 | San Diego, CA, USA